Radiation Oncology

RESEARCH Open Access

Dosimetric investigation of multi-parametric 4D-MRI for radiotherapy in liver cancer

Sha Li[1,2†], Xianggao Zhu[2,3†], Haonan Xiao[4], Weiwei Liu[2], Yibao Zhang[1,2], Jing Cai[4], Tian Li[4*] and Yanye Lu[1,5*]

Abstract

Background In radiotherapy, inadequate management of organ motion in liver cancer may lead to inadequate delineation accuracy, resulting in the underdosage of target tissues and overdosage of surrounding normal tissues. To investigate the clinical potential of multi-parametric 4D-MRI in the target delineation and dose accuracy for liver cancer radiotherapy.

Methods Twenty patients receiving radiotherapy for liver cancer were enrolled. Each patient underwent contrast-enhanced planning CT (free-breathing), contrast-enhanced T1-weighted (free-breathing), T2-weighted (gated) 3D-MRI, and low-quality 4D-MRI using the time resolved imaging with interleaved stochastic trajectories volumetric interpolated breath-hold examination (TWIST-VIBE) sequence. A dual-supervised deformation estimation model was used to generate a 4D deformable vector field (4D-DVF) from 4D-MRI data, and the prior images were deformed using this 4D-DVF to generate multi-parametric 4D-MRI. Assisted by 3D-MRI and multi-parametric 4D-MRI, target contours were performed on the planning CT, resulting in the generation of Target_3D and Target_4D. Clinical plans, Plan_3D and Plan_4D, were designed based on these contours respectively. To explore the dosimetric variations resulting from different contours without re-optimization, Plan_3D was directly applied to Target_4D, and Plan_4D was applied to Target_3D to generate Plan_3D′ and Plan_4D′ respectively. Target volume, contours, dose-volume histograms (DVHs), conformity index (CI), homogeneity index (HI), maximum and mean dose to organ as risks (OARs) were compared and evaluated.

Results Mean volume differences between Target_3D and Target_4D were 2.76 cm^3 (standard deviation [SD] 3.42 cm^3) in the caudate lobe, 181.54 cm^3 (SD 68.50 cm^3) in the left hepatic lobe, and 26.08 cm^3 (SD 20.52 cm^3) in the right hepatic lobe. Mean and SD of CI and HI is 1.02 ± 0.04 and 0.108 ± 0.02 in Plan_3D, 1.02 ± 0.01 and 0.107 ± 0.01 in Plan_4D. There were no statistically significant differences in OAR doses between Plan_3D and Plan_3D′, between Plan_4D and Plan_4D′. However, a statistically significant difference in target dose was observed between Plan_3D and Plan_3D′ ($P = 1.47 \times 10^{-7}$) and between Plan_4D and Plan_4D′ ($P = 0.013$). Plan_3D′ meets 100% of the prescription dose covering mean 77.89% (SD 10.13%) of the Targeted_4D volume, while Plan_4D′ covered mean 94.17% (SD 3.12%) of the Targeted_3D volume.

†Sha Li and Xianggao Zhu contributed equally.

*Correspondence:
Tian Li
tianli@polyu.edu.hk
Yanye Lu
yanye.lu@pku.edu.cn

Full list of author information is available at the end of the article

Conclusions 3D image-guided target delineation may be more likely to underestimate target volume and compromise dose coverage, suggesting that using multi-parametric 4D-MRI can provide more precise target contours and enhance target dose coverage.

Keywords Multi-parametric 4D-MRI, Liver cancer, Radiotherapy, Target contouring, Plan, DDEM

Background

Currently, liver cancer ranks as the fourth leading cause of cancer-related deaths globally [1–3]. The incidence and mortality rates of liver cancer have shown a concerning growth, with a 27% increase in incident cases and a 25% rise in mortality rates between 2010 and 2019 [4]. Traditionally, the role of radiotherapy in treating liver cancer has been limited primarily to palliative applications due to the potential risk of radiation-induced liver disease [5]. However, the development of image-guided radiotherapy (IGRT) has enabled stereotactic body radiotherapy (SBRT) to become one of the main treatments for inoperable liver cancer and liver metastases, significantly improving the local control rate of cancer in patients [6–7]. Despite these advancements, radiotherapy for liver cancer remains a significant challenge due to the respiratory movement of liver [8–9]. Inadequate management of organ motion can negatively affect the distribution of the delivered dose to the irradiated volume, resulting in underdosage of target tissues and overdosage of surrounding normal tissues [10]. Therefore, there is a pressing need for an imaging modality that can visualize tumor motion and improve the accuracy of beam delivery to the target.

In clinical practice, four-dimensional computed tomography (4D-CT) serves as the standard imaging technique used for motion management [11–13]. It is used to generate an internal target volume (ITV) [14] either by combining the targets delineated in each respiratory phase or by using a maximum intensity projection image [15, 16]. However, 4D-CT for liver tumor motion management faces challenges due to soft tissue contrast limitations and higher radiation exposure [17]. Conversely, 4D magnetic resonance imaging (4D-MRI), which provides excellent soft-tissue without ionizing radiation, is a promising technique to address these challenges [18].

Existing 4D-MRI techniques, both retrospective and prospective, have their respective drawbacks despite their ability to generate 4D-MRI images. Retrospective approaches [19–22] involve continuous image acquisition across the entire region of interest (ROI) and subsequent sorting into respiratory phases. However, these sorting algorithms are highly sensitive to patients' irregular breathing patterns, often resulting in image artifacts and compromised image quality. On the other hand, prospective 4D-MRI can be achieved through fast 3D acquisition or respiratory-gated 2D acquisition [23–24]. While this addresses the sorting issue, it typically requires longer scan times, and the problem of image quality persists. Consequently, in current clinical practice, to obtain images with respiratory motion range and high resolution within a shorter timeframe, existing methods typically employ contrast-enhanced planning CT scans, contrast-enhanced T1-weighted (free-breathing) MRI scans, and T2-weighted MRI scans (gated at 20% of end of inhalation and end of exhalation). However, this method fails to reflect the respiratory cycle but only captures instantaneous respiratory states.

To address the limitations of current clinical methods, Xiao et al. introduced an ultra-quality (UQ) 4D-MRI method that uses a novel dual-supervised deformation estimation model (DDEM) based on a commercially available low-quality (LQ) 4D-MRI sequence [25]. This method successfully generated T1-weighted and T2-weighted multi-parametric 4D-MRI images, enhancing image quality and a tumor motion. This method could potentially address the deficiencies of existing 4D-MRI techniques. However, the clinical applicability of this technique is still unknown. To further explore the clinical applicability of multi-parametric 4D-MRI in liver cancer radiotherapy, we explored the application of multi-parametric 4D-MRI images on tumor contouring and radiotherapy planning. This study aims to determine whether multi-parametric 4D-MRI can provide more precise target contours and improve target dose coverage compared to existing methods.

Methods

The workflow of this study is illustrated in Fig. 1. This study begins with the preparation of patient images. Then, with the assistance of 3D-MRI and 4D-MRI, the targets are delineated on the planning CT, generating Target_3D and Target_4D, respectively. Clinical plans, Plan_3D and Plan_4D, are then designed based on these contours. To explore the dosimetric variations caused by different contours without re-optimization, Plan_3D is directly applied to Target_4D, and Plan_4D is applied to Target_3D, generating Plan_3D' and Plan_4D', respectively. Finally, the target delineation and plan quality are evaluated. Specifically, guided by 3D-MRI and 4D-MRI, the delineation effect is assessed by analyzing the differences in tumor target volumes and contours in different liver lobes. Similarly, a dosimetric evaluation is conducted, focusing on target dose and organ-at-risk dose. The detailed methods and steps are described in the following text.

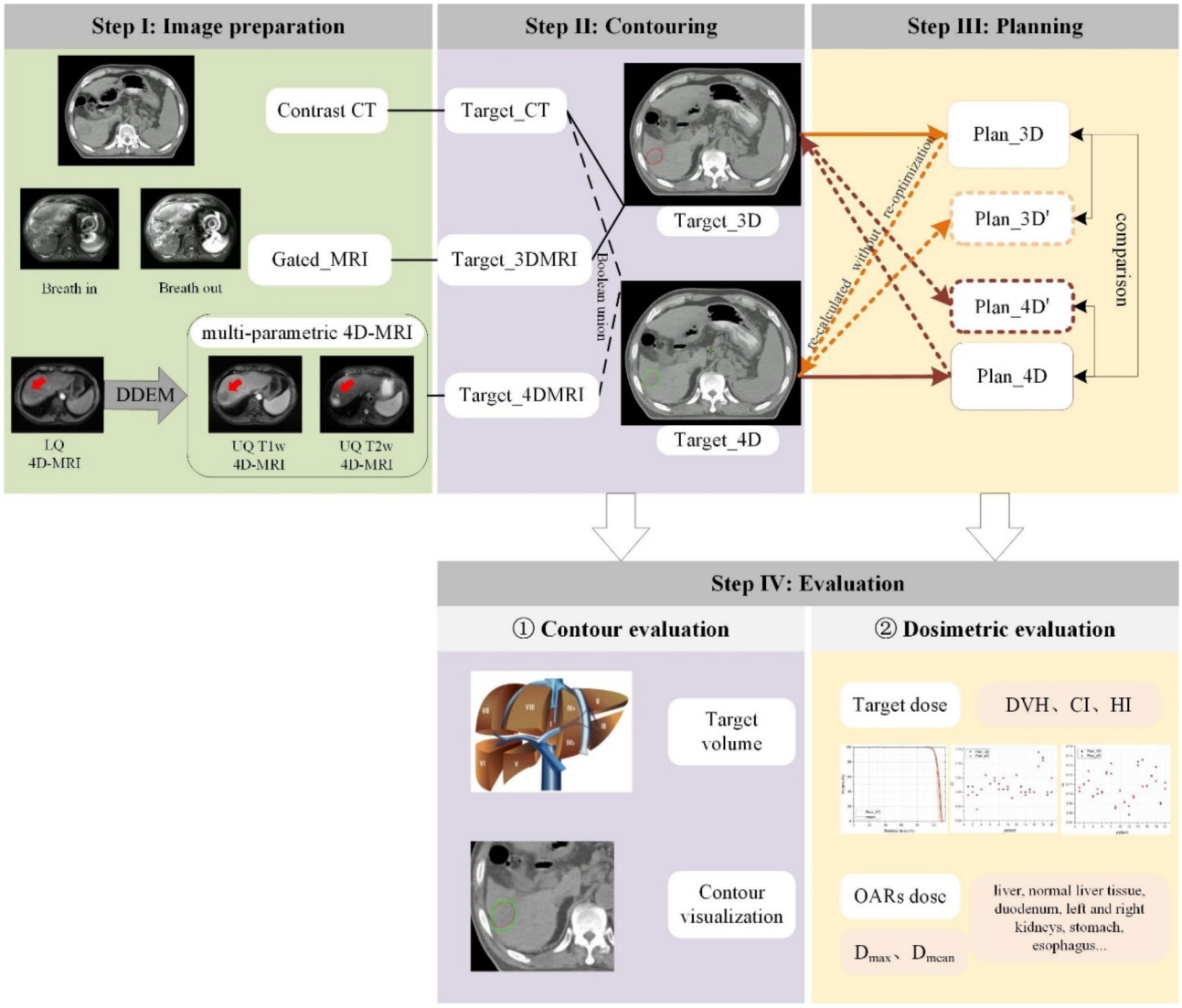

Fig. 1 The workflow of this study

Patient data

The study protocol was approved by the institutional review board. The data utilized in this study were obtained from 20 patients undergoing radiotherapy for liver tumors. Among the 20 patients, 17 were male, and 3 were female. Eighteen patients were diagnosed with primary liver cancer, and two patients were diagnosed with liver metastases. Their average age at diagnosis was 60.4 ± 9.2 years.

The inclusion criteria for patients are as follows: (1) patients receiving radiotherapy for liver tumors; (2) possessing contrast-enhanced planning CT (free-breathing), contrast-enhanced T1-weighted (free-breathing), T2-weighted (gated) 3D-MRI, and low-quality 4D-MRI images, all of which are required.

Image acquisition

The free breathing contrast-enhanced CT images were acquired by a CT scanner (Sensation Open, Siemens, Erlangen, Germany) with the acquisition parameters are as follows: matrix = 512 × 512, thickness = 3 mm, tube current = 146 mA, kVp = 120 kV, while all the MRI scans were performed on a 3.0T scanner (Skyra, Siemens, Erlangen, Germany). Each patient underwent 4D-MRI using the time resolved imaging with interleaved stochastic trajectories (TWIST) volumetric interpolated breath-hold examination (TWIST-VIBE) MRI sequence, which utilized view sharing technique with 20% central region and 20% sampling density in the peripheral region. This commercially available sequence was initially designed for fast volumetric imaging rather than 4D imaging. As in Xiao's study, the acquisition time was reduced to 0.69 s and continuously acquired 72 3D frames to achieve a

4D-MRI scan. Each patient also underwent regular T1w (free-breathing) and T2w (breath-holding) 3D MRI scans. Details of MRI imaging parameters are listed in Table 1. A dual-supervised deformation estimation model was used to generate a 4D deformable vector field (4D-DVF) from 4D-MRI data, and the prior images were deformed using this 4D-DVF to generate multi-parametric 4D-MRI [25].

Contouring

All the target delineation was performed by an experienced radiation oncologist with 15 years of experience. Target_CT was obtained by contouring the target on the planning CT images. Target delineation on the gated T2-weighted on both end of inhalation and end of exhalation was denoted as Target_3DMRI. Subsequently, the clinical target volume Target_3D was generated by performing a Boolean union operation on Target_3DMRI and Target_CT. The contours delineated on all the 10 phases of multi-parametric 4D-MRI are denoted as Target_F0 - Target_F9. Similarly, Target_4DMRI was generated by Boolean union operation on Target_F0 - Target_F9. Likewise, Target_4D was created by performing a Boolean union operation on Target_4DMRI and Target_CT. The naming conventions for targets in different modality images are described in Fig. 1's Step II. Finally target contours and composite volumes of 3D&4D techniques were compared. Organs at risk (OARs) were contoured on CT scans, and the constraints were determined according to the 2022 UK consensus, supplemented with guidelines from the American Society for Radiation Oncology (ASTRO) [26–28]. All the delineations are ultimately presented on the CT images, and the planning design is based on the CT images.

Moreover, based on the widely adopted the Couinaud classification system of liver anatomy internationally, the target locations of 20 patients were categorized. The Couinaud classification system divided the liver into eight independent units (termed segments), including the caudate lobe (segment I), the left hepatic lobe (segments II-IV) and the right hepatic lobe (segments V-VIII). Tumors are positioned in the caudate lobe for 2 patients, while 3 patients had tumors in the left hepatic lobe, and 15 patients exhibited tumor growth in the right hepatic lobe. The eight segments and tumor distributions of 20 patients are shown in Fig. 2. The absolute and percentage volume differences of Target_3D and Target_4D in various hepatic lobes was compared.

Radiotherapy planning

As shown in Fig. 1 in the radiotherapy planning step, the orange and red solid lines indicate that based on Target_3D and Target_4D, two separate radiotherapy plans, Plan_3D and Plan_4D, were created. To evaluate the impact of different target contouring on the plan, Plan_3D was duplicated onto Target_4D and the dose was re-calculated without re-optimization to generate Plan_3D'. Similarly, Plan_4D was copied onto Target_3D and the dose was re-calculated to generate Plan_4D'. These steps are marked by the orange and red dashed lines in Fig. 1 Step III.

All patients underwent intensity modulated radiotherapy (IMRT) or volumetric modulated arc therapy (VMAT) planning on the Varian Eclipse version 15.6 treatment planning system. Among them, seventeen

Table 1 Imaging parameters of MRI

	4D-MRI	**3D-MRI**	
	LQ 4D-MRI	**T1WI**	**T2WI**
Contrast-enhanced	No	Yes	No
Acquisition mode	Free breathing	Free breathing	Gated
Sequence	TWIST-VIBE	Star-VIBE	TSE
Fat suppression	not applicable (N/A)	SPAIR	SPAIR
Turbo factor	N/A	N/A	43
Flip angle (o)	5	9	72
Echo trains per slice	N/A	N/A	6
Parallel imaging (factor)	CAIPIRINHA (4)	N/A	GRAPPA
Acceleration factor (PE)	2	N/A	3
Partial Fourier	6/8	7/8	N/A
TR (ms)	3.44	2.83	1090
TE (ms)	1.23/2.45	1.48	84
Bandwidth (Hz/pixel)	1420	820	781
Matrix size	160 × 128 × 64	320 × 320 × 72	256 × 256 × 40
Voxel size (mm)	2.7 × 2.7 × 2.7	1.2 × 1.2 × 3.0	1.5 × 1.5 × 5.0
Acquisition time	0.69 s per 3D frame	173 s	60 s
Number of frames	72	N/A	N/A

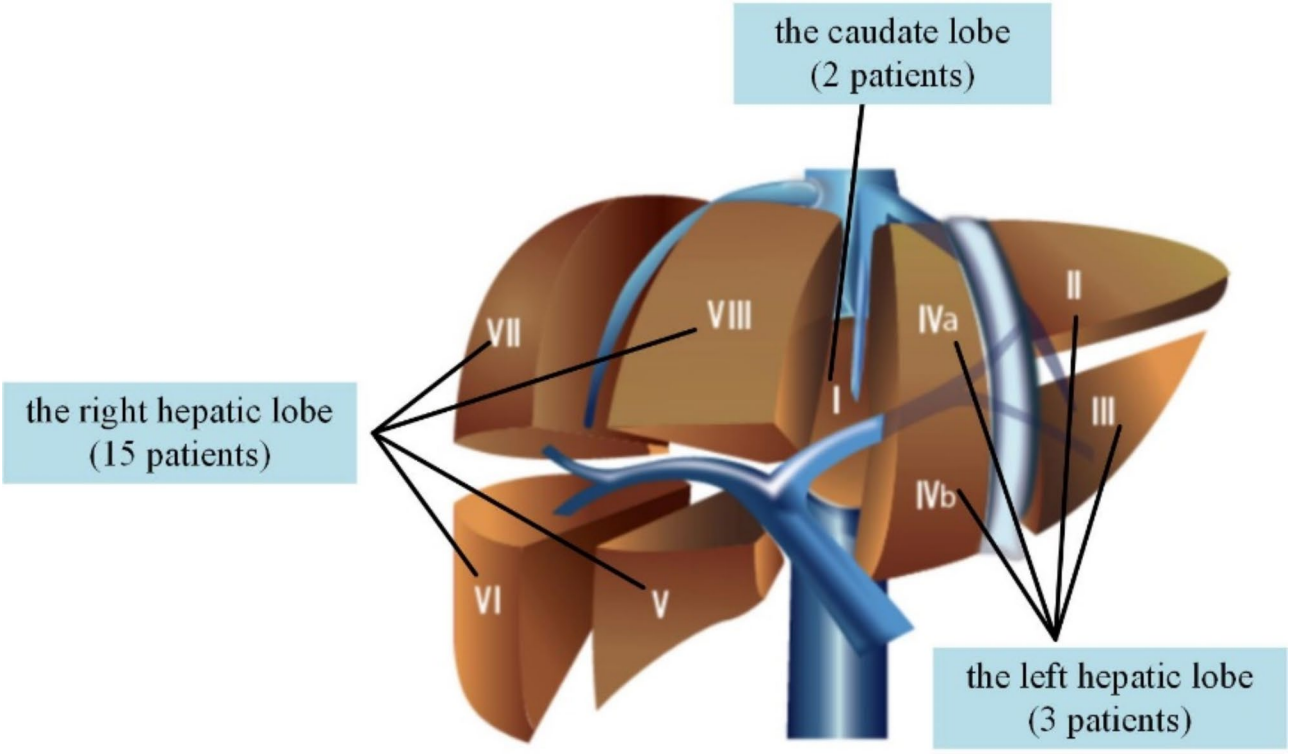

Fig. 2 The couinaud classification system and the tumor distributions of 20 patients

patients received conventional radiotherapy with a prescribed dose of 45 to 56 Gy, administered at 1.8 to 3 Gy per fraction, once daily, five fractions per week. Three patients received SBRT with a dose of 7.5 to 10 Gy per session, administered once daily, five times per week, for a total of 5 to 8 sessions.

For Plan_3D and Plan_4D, the target dose distribution is evaluated using the conformity index (CI) and homogeneity index (HI) as defined in the ICRU83 report [29]. The calculation formulas are as follows:

$$HI = (D_{2\%} - D_{98\%})/D_{50\%} \quad (1)$$

$$CI = V_{100\%Rx}/V_{target} \quad (2)$$

where $D_{x\%}$ indicates the dose to $x\%$ of the volume, $V_{100\%Rx}$ and V_{target} indicate the volumes receiving at least 100% of the prescribed dose and the target volumes respectively.

Statistical methods

Statistical analysis of the target volumes was performed using SPSS (v21.0, IBM Analytics, Armonk, NY). The Shapiro-Wilk method was employed to test the normality of the target volume distribution. For normally distributed data, the T-test was used, while the Mann-Whitney test was utilized for non-normally distributed data. Both tests were conducted as two-tailed tests with a significance level of 0.05.

Results

Target volume

The measured target volume on different image modalities is shown in Table 2. The comparison of the average target volumes between 3D-MRI and 4D-MRI showed no statistically significant difference ($P = 0.355$). Similarly, there was no statistically significant difference in target volumes between Target_3D and Target_4D ($P = 0.398$).

Contour visualization

There are two patients whose tumors are located in the caudate lobe, and the target volume in this region is minimally affected by respiration (Fig. 3a). The mean volume difference between Target_3D and Target_4D is 2.76 cm^3 (SD 3.42 cm^3), with the average percentage volume difference of 22% (SD 17%). Tumors not near rigid structures such as the chest wall and spinal cord are more influenced by respiratory, visceral, and dietary movements, resulting in a greater difference between Target_3D and Target_4D, especially when the tumor is close to the diaphragm apex. In the left hepatic lobe (Fig. 3b), the mean absolute and percentage volume differences are 181.54 cm^3 (SD 68.50 cm^3) and 30% (SD 3%). Due to the constraint of the chest wall, the target area in the right hepatic lobe is also subject to limited impact from respiration (Fig. 3c). The mean absolute and percentage volume differences in the right hepatic lobe are 26.08 cm^3 (SD 20.52 cm^3) and 21% (SD 14%). Figure 3 displays the

Table 2 Target volumes in different modal images [cm^3]

		CT	MRI		MRI registration to CT	
		Target_CT	**Target_3DMRI**	**Target_4DMRI**	**Target_3D**	**Target_4D**
Mean		108.56	120.94	172.87	144.98	192.05
SE		23.83	28.25	39.68	31.85	45.11
SD		106.58	126.34	177.46	142.44	201.75
95% CI	lower	58.68	61.80	89.82	78.32	97.63
	upper	158.44	180.07	255.93	211.65	286.47
Median		65.29	80.36	122.21	91.20	123.24
P		-	0.355		0.398	

Note: SE = standard error, SD = standard deviation, 95% CI = 95% confidence interval

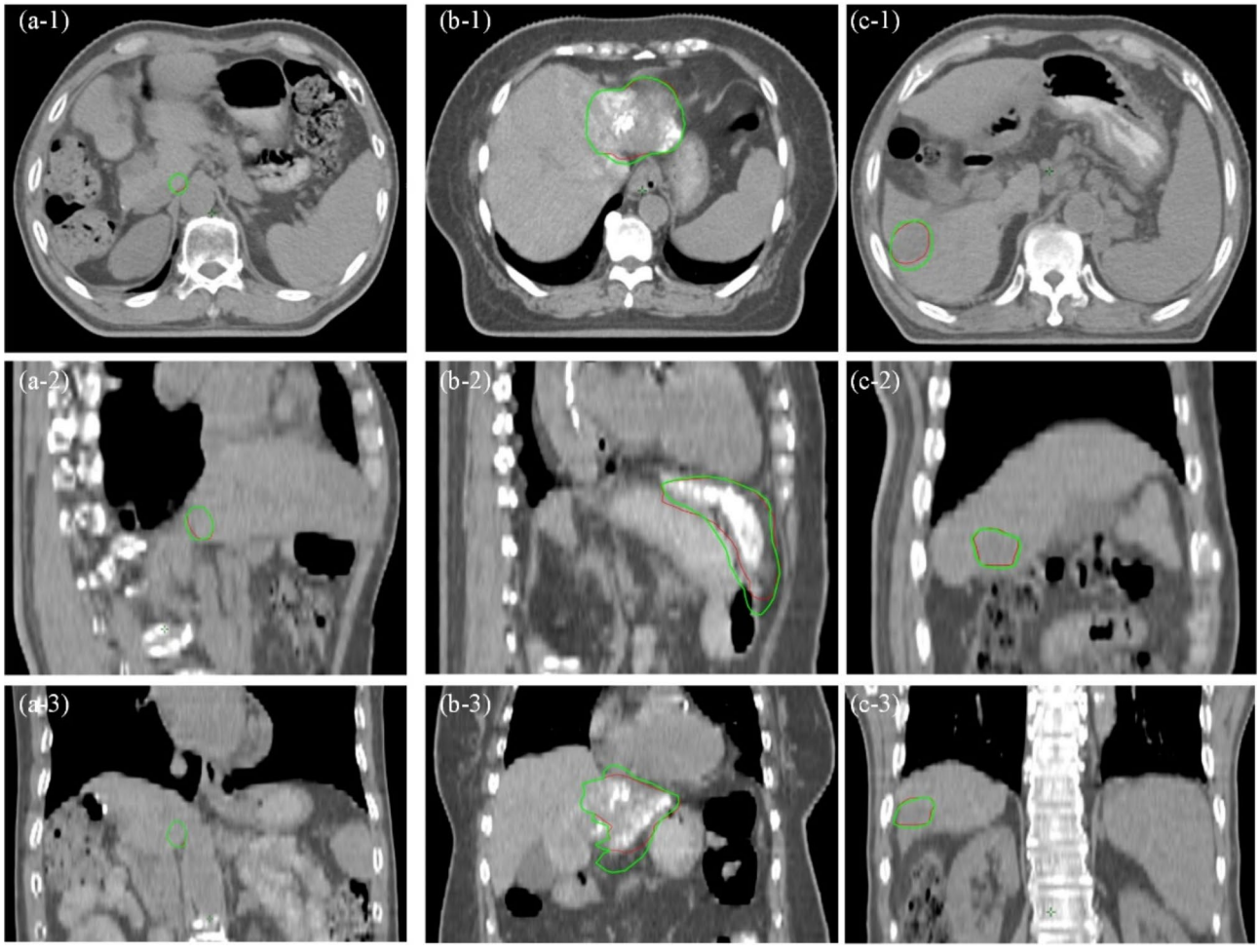

Fig. 3 Three examples of target contouring in transversal **(-1)**, sagittal **(-2)**, and frontal **(-3)** views. The green line is Target_4D based on multi-parametric 4D-MRI and paired CT, and the red line is Target_3D drawn based on 3D-MRI and paired CT

target contours of three patients in three different hepatic lobes.

Target dose

All Plan_3D and Plan_4D meet 100% of the prescription dose covering at least 95% of the target volume (Fig. 4a and b). In Plan_3D, the mean Target_3D volume of 96.02% (SD 0.61%) could meet 100% of the prescription dose. In Plan_4D, plans meet 100% of the prescription dose covering mean 95.98% (SD 0.53%) of the Target_4D volume. There was no statistically significant difference between Plan_3D and Plan_4D ($P = 0.82$).

When Plan_3D was copied to Target_4D, 95% of the Target_4D volume could not be reached to the prescription dose, with the exception of one case where the tumor located in the caudate lobe and volume were less

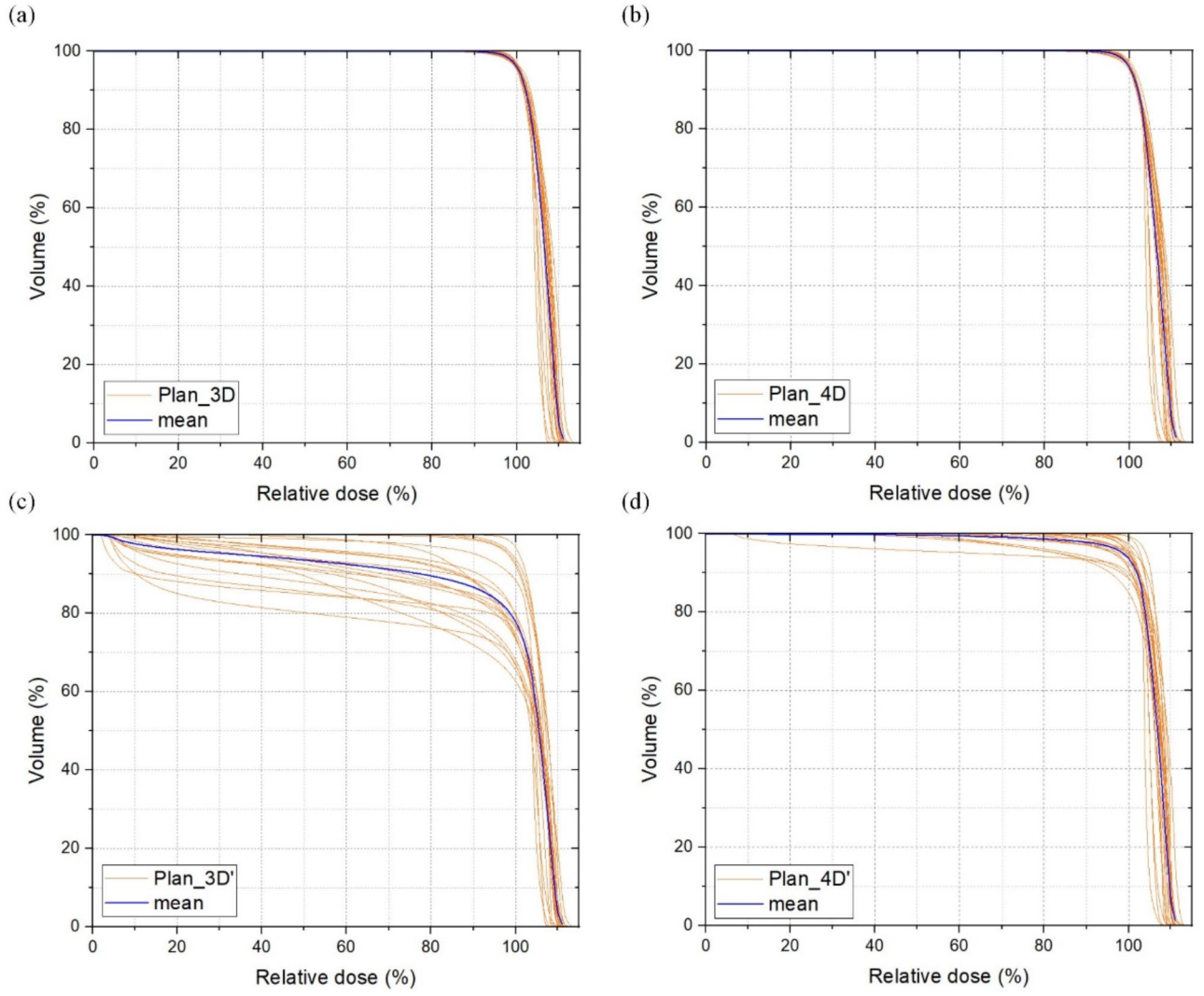

Fig. 4 The target dose-volume histograms (DVHs) of 20 patients. (**a**) is Plan_3D. (**b**) is Plan_4D. (**c**) and (**d**) are Plan_3D' and Plan_4D', respectively

affected by respiratory movement and were not adjacent to the lung (Fig. 4c). Another tumor located in the caudate lobe reached 100% of the prescription dose by 93.94% volume. Plan_3D' meets 100% of the prescription dose covering mean 77.89% (SD 10.13%) of the Target_4D volume. There was statistically significant difference between Plan_3D and Plan_3D' ($P = 1.47 \times 10^{-7}$). When Plan_4D was copied to Target_3D, plans meet 100% of the prescription dose covering mean 94.17% (SD 3.12%) of the Target_3D volume (Fig. 4d). There was statistically significant difference between Plan_4D and Plan_4D' ($P = 0.013$).

In Plan_3D, the mean and SD of CI for the 20 patients is 1.02 ± 0.04 (95%CI [1.01 1.05]), and HI is 0.108 ± 0.02 (95%CI [0.100 1.15]). The mean and SD of CI for the 20 patients in Plan_4D is 1.02 ± 0.01 (95%CI [1.00 1.04]), and HI is 0.107 ± 0.01 (95%CI [0.101 1.13]). The specific values of CI and HI for the 20 patients are shown in Fig. 5. The comparison of CI and HI between Plan_3D and Plan_4D showed no statistically significant difference (P_{CI} = 0.718, P_{HI} = 0.878).

OARs dose

The analysis of dose to OARs was performed, including the maximum dose in the spinal cord and duodenum, as well as the mean dose in several organs, including the liver, normal liver tissue, duodenum, left and right kidneys, stomach, and esophagus. The results can be found in Table 3 and no statistically significant difference in OAR doses was found between Plan_3D and Plan_3D', Plan_4D and Plan_4D'.

Discussion

Respiration is the main source of motion for abdominal tumors. Respiratory-induced displacements can extend to several centimeters in the cranio-caudal (CC) direction

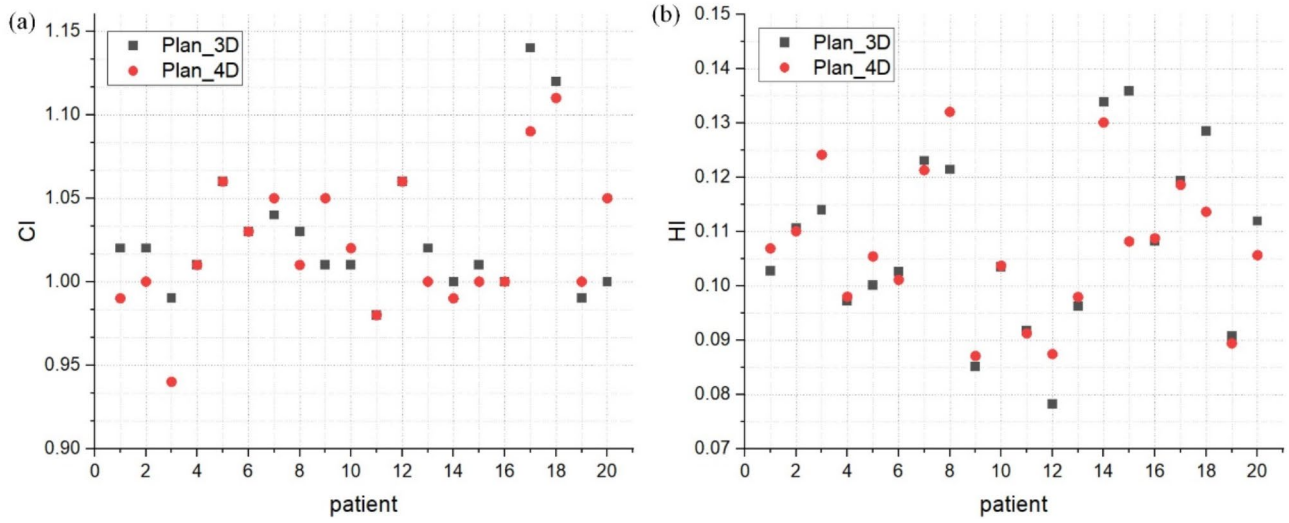

Fig. 5 CI and HI maps of 20 patients. (**a**) represents the CI map for the 20 patients, while (**b**) represents the HI map. The gray box represents Plan_3D, and the red circle represents Plan_4D

Table 3 OARs dose in Plan_3D, Plan_3D', Plan_4D and Plan_4D' [cGy]

	Plan_3D	Plan_3D'	Plan_4D	Plan_4D'
SpinalCord				
D_{max}	1360.0 ± 850.8	1360 ± 850.1	1357.7 ± 909.8	1358.4 ± 911.2
p	1.000		0.998	
liver				
D_{mean}	1671.2 ± 711.6	1671.2 ± 711.6	1854.6 ± 763.7	1854.7 ± 763.7
p	1.000		1.000	
Normal liver				
D_{mean}	1027.4 ± 449.1	1012.3 ± 454.1	1194.3 ± 513.8	1257.3 ± 513.5
p	0.917		0.7	
Duodenum				
D_{max}	1731.3 ± 1803.1	1731.6 ± 1803.0	2399.1 ± 2107.5	2399.6 ± 2107.2
p	0.986*		0.972*	
D_{mean}	470.5 ± 712.7	470.5 ± 712.7	689.0 ± 860.60	688.9 ± 860.7
p	0.986*		0.972*	
Kidney_L				
D_{mean}	88.9 ± 148.2	87.1 ± 149.0	138.7 ± 216.7	138.7 ± 216.7
p	0.849*		1.000*	
Kidney_R				
D_{mean}	213.6 ± 374.2	209.9 ± 375.2	279.1 ± 439.9	279.1 ± 439.8
p	0.965*		0.988*	
Stomach				
D_{mean}	921.4 ± 1070.3	921.4 ± 1070.3	1103.3 ± 1359.2	1103.3 ± 1359.3
p	1.000*		0.988*	
Esophagus				
D_{mean}	1342.6 ± 1197.5	1342.6 ± 1197.5	1456.3 ± 1323.4	1456.4 ± 1323.3
p	0.985*		0.985*	

Note: D_{max} and D_{mean} are the maximum and mean dose of the structure, respectively. * indicates the Mann-Whitney test; Otherwise, t-test is performed

[30, 31]. Tumor positions and shapes can vary substantially across time points. Underestimating target volume compromises dose coverage, while overestimating it leads to unnecessary OAR radiation and elevated toxicity risk [32]. Therefore, characterizing respiratory-induced motion of the tumor and OARs is vital to minimize radiation toxicity to healthy tissue and maximize the target dose during radiotherapy. Although 4D-CT remains the standard imaging technique used for motion management, its application in abdominal cancer is limited by

insufficient soft-tissue contrast and additional ionizing radiation. In contrast, 4D-MRI offers versatile soft-tissue contrast without ionizing radiation [18, 33]. Therefore, 4D-MRI holds great potential in abdominal tumor motion management.

Chen et al. [34] evaluated the feasibility of 4D-MRI in the target delineation of primary liver cancer. Compared with 4D-CT, T2-weighted and navigator-triggered 4D-MRI demonstrated fewer artifacts and more accurate motion assessment, potentially reducing the uncertainty in target delineation. While this study demonstrated 4D-MRI's potential for liver cancer targeting, its dose advantages in target delineation weren't evaluated. Additionally, the 4D-MRI used in this study had a slice thickness of 5 mm. For patients requiring SBRT, the slice thickness of 3 mm or thinner is preferred, yet maintaining both scanning efficiency and image quality becomes challenging. Zhang et al. [35] also explored clinical utility of 4D-MRI for lung tumor delineation and motion assessment. This study showed that 4D-MRI is a promising and viable technique for clinical lung tumor delineation and motion assessment. Similarly, the study did not explore the dosimetric impact of target contouring and faced challenges related to scanning time and image quality. In contrast, the multi-parametric 4D-MRI technique used in this study provides improved spatial-temporal resolution within a clinically acceptable scanning time compared to the 4D-MRI technique used in aforementioned studies, presenting great potential for precise tumor motion management.

Upon acquiring 4D scans, the subsequent challenge is the application in treatment planning. In this study, we explored the clinical applicability of multi-parametric 4D-MRI in liver cancer radiotherapy. We statistically analyzed target volume and contour changes and explored the dosimetric impacts. While no significant target volume differences between Target_3D and Target_4D were noted, contour variations were evident. In the 4D-MRI datasets, there was an increase in tumor volume (192.05 cc compared to 144.98 cc), even though the 3D-MRI datasets considered both maximum inhalation and exhalation phases. The possible reasons for this phenomenon are as follows: 3D-MRI scans are performed at a specific time point, reflecting the tumor's morphology at that moment. In contrast, 4D-MRI scans are taken at multiple time points, considering the tumor's dynamic behavior at different stages of the respiratory cycle. Therefore, with 4D-MRI data, doctors may identify more tumor regions, especially when the tumor's contour changes due to breathing. Additionally, 4D-MRI captures the tumor's state at different time points during the respiratory process. Breathing not only leads to changes in the tumor's position but also alters its shape and volume during inhalation and exhalation. Since 4D-MRI can capture these dynamic changes, it may show the tumor's maximum volume throughout the entire respiratory cycle. A larger average volume from Target_4D implies superior target coverage potential for motion-affected tumors, thereby enabling better tumor control. From a dosimetric perspective, using 3D-MRI for tumor delineation could underdose the target, consistent with previous studies [32, 36]. For OARs, a larger tumor volume may increase the risk of radiation, especially when the tumor is located near the OARs. As shown in the results of Tables 3 and 4D-MRI results in a higher mean radiation dose to the normal liver, stomach, kidneys, and duodenum compared to 3D-MRI. We recommend further optimizing dose distribution in future radiotherapy plans to minimize radiation exposure to normal tissues.

Although no significant target volume differences between Target_3D and Target_4D were found, gated MRI could be affected by respiratory control and patient-specific factors, influencing contour outcomes. Yu et al. [37] have demonstrated that approximately 5 mm anatomical landmark positional differences in all directions were found between gated MRI and 4D-CT fusion planning for hepatocellular carcinoma patients; the gap was larger in patients with ascites or pulmonary disease. The magnitude of respiratory motion impact is directly correlated with the delineation differences between the 3D and 4D images.

In this study, Table 2 shows a 32.47% mean volume increase in Target_4D compared to Target_3D, aligning with reasonable expectations. For example, Xu et al. [32] illustrates that the motion of the GTV varies from − 4.4 to 177% from 4D-CT to 4D-MRI. The volume changes between Target_3D and Target_4D in different liver lobes ranked from largest to smallest as follows: left hepatic lobe, right hepatic lobe and caudate lobe. The reason is that tumors in the left hepatic lobe are not close to rigid structures such as spinal cord, which makes them susceptible to the influence of respiratory, visceral, and dietary movements, especially at the apex of the diaphragm. The right liver lobe is constrained by the chest wall, resulting in limited tumor movement. Meanwhile, the caudate lobe is located near the spine and major blood vessels, which is why tumors in this hepatic lobe are least affected by respiration [38].

In Fig. 4**(d)**, seven plans failed to meet the requirement of 95% of the target volume with prescribed dose. The possible reasons are: 1) Gated technique may introduce some uncertainty in tumor delineation [39, 40]. For example, respiration-gated scanning can be performed using external surrogates, but the correlation between such surrogates and tumor motion may vary [40]. 2) Target_4D and Target_3D does not represent a simple relationship of inclusion and being included. 3) These cases, mostly diaphragm-proximal tumors, were

significantly impacted by respiratory motion, particularly in the CC direction [41]. Additionally, proximity to the lungs introduces complexities in dose calculations, resulting in dosimetric discrepancies on the DVH [42]. Although the dosimetric difference between Plan_3D & Plan_3D' and Plan_4D & Plan_4D' are statistically significant ($P = 1.47 \times 10^{-7}$, $P = 0.013$), Plan_3D' meets 100% of the prescription dose covering mean 77.89% (SD 10.13%) of the target volume, and Plan_4D' covered mean 94.17% (SD 3.12%) of the target volume. This suggests that the 3D image-guided target delineation may be more likely to underestimate target volume and compromise dose coverage.

Notwithstanding the promising results of multi-parametric 4D-MRI, the study does have certain limitations. One limitation of our study is the temporal resolution of multi-parametric 4D-MRI, which may warrant future improvements by reducing acquisition times of the original commercial 4D-MRI scans. Some studies have demonstrated the feasibility of deformable vector field estimation using highly under sampled images and this could potentially be utilized in optimizing the multi-parametric 4D-MRI [43]. Another limitation lies in the absence of 4D-CT images. Lastly, due to the labor-intensive and time-consuming nature of contouring targets across various modality images and phases, only 20 hepatocellular carcinoma cases were included in the clinical testing. Future endeavors will aim to enroll a larger cohort of patients.

Conclusion

In conclusion, our research study underscores the potential value and significance of multi-parametric 4D-MRI in the domain of liver cancer radiotherapy. By optimizing tumor delineation and dosimetric precision, the integration of multi-parametric 4D-MRI holds promise in advancing treatment outcomes and patient care in liver cancer radiotherapy. Future studies on a larger cohort of patients are warranted to further verify the efficacy of multi-parametric 4D-MRI.

Abbreviations

IGRT	Image-guided radiotherapy
SBRT	Stereotactic body radiotherapy
4D-CT	Four-dimensional computed tomography
4D-MRI	4D magnetic resonance imaging
ITV	Internal target volume
ROI	Region of interest
LQ 4D-MRI	Low-quality 4D-MRI
UQ 4D-MRI	Ultra-quality 4D-MRI
TWIST-VIBE	Time resolved imaging with interleaved stochastic trajectories volumetric interpolated breath-hold examination
ASTRO	The American Society for Radiation Oncology
IMRT	Intensity modulated radiotherapy
VMAT	Volumetric modulated arc therapy
OAR	Organs at risk
CI	Conformity index
HI	Homogeneity index

Acknowledgements

The authors thank all physicists and dosimetrists at Beijing Cancer Hospital for their assistance and extend special thanks to Dr. Shuai Li and Dr. Hongzhi Wang for their technical support.

Author contributions

Conception and design: Yanye Lu and Tian Li. Development of methodology and model: Sha Li, Xianggao Zhu and Haonan Xiao. Acquisition of data: Weiwei Liu. Analysis and interpretation of data: Sha Li, Xianggao Zhu and Yibao Zhang. Writing and review of the manuscript: Sha Li, Xianggao Zhu, Yanye Lu and Tian Li. Administrative, technical, or material support: Yanye Lu, Yibao Zhang, Tian Li and Jing Cai.

Funding

This work was jointly supported by NSFC Young Scientists Fund (82202941), the Natural Science Foundation of China (12275012, 623B2001), Foundation of Peking University Cancer Hospital (PY202305, JC202505,PY202306), Beijing Natural Science Foundation (Z210008), Science and Technology Program of the Joint Fund of Scientific Research for the Public Hospitals of Inner Mongolia Academy of Medical Sciences(2023GLLH0138), General Research Fund (GRF 15104822, GRF 15102219), the University Grants Committee, the Health and Medical Research Fund (HMRF 10211606), the Health Bureau, The Government of the Hong Kong Special Administrative Regions, and Innovation and Technology Support Programme (ITS/049/22FP), Innovation and Technology Commission, Hong Kong Special Administrative Regions.

Data availability

No datasets were generated or analysed during the current study.

Declarations

Ethics approval and consent to participate

This study was conducted in accordance with the Declaration of Helsinki and was approved by the Ethics Committee of the Peking University Beijing Cancer Hospital and Institute, and the requirement for individual informed patient consent waived owing to the retrospective nature of the study.

Consent for publication

All authors have agreed on the contents of the manuscript and provided consent.

Competing interests

The authors declare no competing interests.

Author details

[1]Institute of Medical Technology, Peking University Health Science Center, Beijing 100191, China
[2]Key Laboratory of Carcinogenesis and Translational Research (Ministry of Education / Beijing), Department of Radiation Oncology, Peking University Cancer Hospital & Institute, Beijing Cancer Hospital & Institute, Beijing 100142, China
[3]Department of Radiotherapy, Affiliated Cancer Hospital of Inner Mongolia Medical University & Peking University Cancer Hospital (Inner Mongolia Campus); Key Laboratoy of Radiation Physics and Biology of Inner Mongolia Medical University, Huhhot, Inner Mongolia, China
[4]Department of Health Technology and Informatics, The Hong Kong Polytechnic University, Hong Kong SAR, China
[5]National Biomedical Imaging Center, Peking University, Beijing 100871, China

Received: 1 August 2024 / Accepted: 9 February 2025
Published online: 11 April 2025

References

1. Zhou K, Gainey CS, Dodge JL, et al. Diverging incidence trends for hepatocellular carcinoma in rural and urban settings in the United States. Clin Gastroenterol Hepatol. 2021;20(5):1180–5. https://doi.org/10.1016/j.cgh.2021.08.032.

2. Orci LA, Sanduzzi-Zamparelli M, Caballol B, et al. Incidence of hepatocellular carcinoma in patients with nonalcoholic fatty liver disease: a systematic review, meta-analysis, and meta-regression. Clin Gastroenterol Hepatol. 2021;20(2):283–92. https://doi.org/10.1016/j.cgh.2021.05.002.
3. Nagaoki Y, Hyogo H, Ando Y, et al. Increasing incidence of non-HBV- and non-HCV-related hepatocellular carcinoma: single-institution 20-year study. BMC Gastroenterol. 2021;21(1):306. https://doi.org/10.1186/s12876-021-01884-5.
4. Huang DQ, Singal AG, Kono Y, Tan DJH, El-Serag HB, Loomba R. Changing global epidemiology of liver cancer from 2010 to 2019: NASH is the fastest growing cause of liver cancer. Cell Metab. 2022;34(7):969–77. https://doi.org/10.1016/j.cmet.2022.05.003.
5. Chen CP. Role of radiotherapy in the treatment of hepatocellular carcinoma. J Clin Transl Hepatol. 2019;7(2):183–90. https://doi.org/10.14218/JCTH.2018.00060.
6. Gerum S, Heinz C, Belka C, et al. Stereotactic body radiation therapy (SBRT) in patients with hepatocellular carcinoma and oligometastatic liver disease. Radiat Oncol. 2018;13(1):100. https://doi.org/10.1186/s13014-018-1048-4.
7. Rim CH, Kim HJ, Seong J. Clinical feasibility and efficacy of stereotactic body radiotherapy for hepatocellular carcinoma: a systematic review and meta-analysis of observational studies. Radiother Oncol. 2019;131:135–44. https://doi.org/10.1016/j.radonc.2018.12.005.
8. Dhont J, Harden SV, Chee LYS, et al. Image-guided radiotherapy to manage respiratory motion: lung and liver. Clin Oncol. 2020;32(12):792–804. https://doi.org/10.1016/j.clon.2020.09.008.
9. Duncan DB, Johannes KV, Geertjan VT, Arjan B, Zdenko VK. Evaluating differences in respiratory motion estimates during radiotherapy: a single planning 4DMRI versus daily 4DMRI. Radia Onco. 2021;26(16):188–97. https://doi.org/10.1186/s13014-021-01915-1.
10. Lambert J, Suchowerska N, Mckenzie DR, Jackson M. Intra-fractional motion during proton beam scanning. Phys Med Biol. 2005;50(20):4853–62. https://doi.org/10.1088/0031-9155/50/20/008.
11. Keall PJ, Mageras GS, Balter JM, et al. The management of respiratory motion in radiation oncology report of AAPM Task Group 76. Med Phys. 2006;33(10):3874–900. https://doi.org/10.1118/1.2349696.
12. Mageras GS, Pevsner A, Yorke ED, et al. Measurement of lung tumor motion using respiration-correlated CT. Int J Radiat Oncol Biol Phys. 2004;60(3):933–41. https://doi.org/10.1016/j.ijrobp.2004.06.021.
13. Pan T. Comparison of helical and cine acquisitions for 4D-CT imaging with multislice CT. Med Phys. 2005;32(2):627–34. https://doi.org/10.1118/1.1855013.
14. Borm KJ, Oechsner M, Wiegandt M, Hofmeister A, Combs SE, Duma MN. Moving targets in 4D-CTs versus MIP and AIP: comparison of patients data to phantom data. BMC Cancer. 2018;18(1):760. https://doi.org/10.1186/s12885-018-4647-4.
15. Bradley JD, Nofal AN, El Naqa IM, et al. Comparison of helical, maximum intensity projection (MIP), and averaged intensity (AI) 4D-CT imaging for stereotactic body radiation therapy (SBRT) planning in lung cancer. Radiother Oncol. 2006;81(3):264–8. https://doi.org/10.1016/j.radonc.2006.10.009.
16. Chan M, Chiang CL, Lee V, et al. Target localization of 3D versus 4D cone beam computed tomography in lipiodol-guided stereotactic radiotherapy of hepatocellular carcinomas. PLoS ONE. 2017;12(4):e0174929. https://doi.org/10.1371/journal.pone.0174929.
17. Li T, Schreibmann E, Thorndyke B, et al. Radiation dose reduction in four-dimensional computed tomography. Med Phys. 2005;32(12):3650–60. https://doi.org/10.1118/1.2122567.
18. Stemkens B, Paulson ES, Tijssen RH. Nuts and bolts of 4D-MRI for radiotherapy. *Phys Med Biol.* 2018;63(21): 21TR01. https://doi.org/10.1088/1361-6560/aae56d
19. Yang J, Cai J, Wang H, et al. Is diaphragm motion a good surrogate for liver tumor motion? Int J Radiat Oncol Biol Phys. 2014;90(4):952–8. https://doi.org/10.1016/j.ijrobp.2014.07.028.
20. Yang J, Cai J, Wang H, et al. Four-dimensional magnetic resonance imaging using axial body area as respiratory surrogate: initial patient results. Int J Radiat Oncol Biol Phys. 2014;88(4):907–12. https://doi.org/10.1016/j.ijrobp.2013.11.245.
21. Liu Y, Yin F-F, Chen N-k, Chu M-L, Cai J. Four-dimensional magnetic resonance imaging with retrospective k-space reordering: a feasibility study. Med Phys. 2015;42(2):534–41. https://doi.org/10.1118/1.4905044.
22. Keijnemans K, Borman PTS, van Lier A, Verhoeff JJC, Raaymakers BW, Fast MF. Simultaneous multi-slice accelerated 4D-MRI for radiotherapy guidance. Phys Med Biol. 2021;66(9). https://doi.org/10.1088/1361-6560/abf591.
23. Yuan J, Wong OL, Zhou Y, Chueng KY, Yu SK. A fast volumetric 4D-MRI with sub-second frame rate for abdominal motion monitoring and characterization in MRI-guided radiotherapy. Quant Imaging Med Surg. 2019;9(7):1303–14. https://doi.org/10.21037/qims.2019.06.23.
24. Li G, Wei J, Olek D, et al. Direct comparison of respiration correlated four-dimensional magnetic resonance imaging reconstructed using concurrent internal navigator and external bellows. Int J Radiat Oncol Biol Phys. 2017;97(3):596–605. https://doi.org/10.1016/j.ijrobp.2016.11.004.
25. Xiao HN, Ni RY, Zhi SH, et al. A dual-supervised deformation estimation model (DDEM) for constructing ultra-quality 4D-MRI based on a commercial low-quality 4D-MRI for liver cancer radiation therapy. Med Phys. 2022;49(5):3159–70. https://doi.org/10.1002/mp.15542.
26. Diez P, Hanna GG, Aitken KL, et al. UK 2022 Consensus on normal tissue dose-volume constraints for Oligometastatic, primary lung and Hepatocellular Carcinoma Stereotactic Ablative Radiotherapy. Clin Oncol. 2022;34(5):288–300. https://doi.org/10.1016/j.clon.2022.02.010.
27. Smith A, Aisling B, Minsong C, et al. External Beam Radiation Therapy for Primary Liver cancers: an ASTRO Clinical Practice Guideline. Practical Radiation Oncol. 2022;12(1):28–51. https://doi.org/10.1016/j.prro.2021.09.004.
28. Wang H, Zheng X, Sun J, et al. 4D-MRI assisted stereotactic body radiation therapy for unresectable colorectal cancer liver metastases. Clin Transl Radiat Oncol. 2023;45:100714. https://doi.org/10.1016/j.ctro.2023.100714.
29. U.S.A. International commission on radiation units and measurements. ICRU 83 prescribing recording, and reporting photon-beam IMRT technical report. 7010 Woodmont Avenue Bethesda, Maryland 20814. (2010).
30. Heerkens HD, van Vulpen M, van den Berg CAT, et al. MRI-based tumor motion characterization and gating schemes for radiation therapy of pancreatic cancer. Radiother Oncol. 2014;111(2):252–7. https://doi.org/10.1016/j.radonc.2014.03.002.
31. Von Siebenthal M, Szekely G, Gamper U, Boesiger P, Lomax A, Cattin P. 4D MR imaging of respiratory organ motion and its variability. Phys Med Biol. 2007;52(6):1547–64. https://doi.org/10.1088/0031-9155/52/6/001.
32. Xu L, Nie X, Zhang L et al. Tumor motion and dosimetry variability based on 4DMRI in comparison with 4DCT. 61st Annual Meeting of the American Society for Radiation Oncology (*ASTRO)*. 2019; E757. https://doi.org/10.1016/j.ijrobp.2019.06.784
33. Xiao H, Han X, Zhi S, et al. Ultra-fast multi-parametric 4D-MRI image reconstruction for real-time applications using a downsampling-invariant deformable registration (D2R) model. Radiother Oncol. 2023;189:109948. https://doi.org/10.1016/j.radonc.2023.109948.
34. Chen YK, Gong GG, Wang YX, et al. Comparative evaluation of 4-dimensional computed tomography and 4-dimensional magnetic resonance imaging to delineate the target of primary liver cancer. Technol Cancer Res Treat. 2021;20:15330338211045499. https://doi.org/10.1177/15330338211045499.
35. Zhang J, Srivastava S, Wang C, et al. Clinical evaluation of 4D MRI in the delineation of gross and internal tumor volumes in comparison with 4DCT. J Appl Clin Med Phys. 2019;20(9):51–60. https://doi.org/10.1002/acm2.12699.
36. Keall P. 4-dimensional computed tomography imaging and treatment planning. Semin Radiat Oncol. 2004;14(1):81–90. https://doi.org/10.1053/j.semradonc.2003.10.006.
37. Yu JI, Kim JS, Park HC, et al. Evaluation of anatomical landmark position differences between respiration-gated MRI and four-dimensional CT for radiation therapy in patients with hepatocellular carcinoma. Br J Radiol. 2013;86(1021):20120221. https://doi.org/10.1259/bjr.20120221.
38. Thomas HR, Miao X, Ferguson D, Calvin C, Bhaskar Krishnamurthy U, Anwar M, Feng M, Scholey J. Contrast-enhanced 4D-MRI for internal target volume generation in treatment planning for liver tumors. Radiother Oncol. 2022;173:69–76. https://doi.org/10.1016/j.radonc.2022.05.037.
39. John R, van Sörnsen de Koste MA, Palacios, Anna ME, Bruynzeel, Ben J, Slotman S, Senan FJ. Lagerwaard, MR-guided gated Stereotactic Radiation Therapy Delivery for Lung, adrenal, and pancreatic tumors: a geometric analysis. Int J Radiat Oncol Biol Phys. 2018;102(4):858–66. https://doi.org/10.1016/j.ijrobp.2018.05.048.
40. Korreman SS. Image-guided radiotherapy and motion management in lung cancer. Br J Radiol. 2015;88(1051):20150100. https://doi.org/10.1259/bjr.20150100.
41. Abdul Ghani MNH, Ng WL. Management of respiratory motion for lung radiotherapy: a review. J Xiangya Med. 2018;3:27–27. https://doi.org/10.21037/jxym.2018.06.03.
42. Lamichhane N, Studenski MT. Improving TBI lung dose calculations: can the treatment planning system help? Med Dosim. 2019;45(2):168–71. https://doi.org/10.1016/j.meddos.2019.09.004.

43. Terpstra ML, Maspero M, D'Agata F, et al. Deep learning-based image reconstruction and motion estimation from under sampled radial k-space for real-time MRI-guided radiotherapy. Phys Med Biol. 2020;65(15):155015. https://doi.org/10.1088/1361-6560/ab9358.

Publisher's note